Journal of Solid State Chemistry **149,** 262–275 (2000)
doi:10.1006/jssc.1999.8526, available online at http://www.idealibrary.com on IDEAL®

Cation Loss of $BaCa_{0.393}Nb_{0.606}O_{2.91}$ in Aqueous Media: Amorphization at Room Temperature

T. Schober,[1] K. Szot, M. Barton, and B. Kessler

Institut für Festkörperforschung (IFF), Forschungszentrum Jülich, 52425 Jülich, Germany

U. Breuer

Zentralabteilung für Chemische Analysen (ZCH), Forschungszentrum Jülich, 52425 Jülich, Germany

H. J. Penkalla

Institut für Werkstoffe und Verfahren der Energietechnik (IWV2), Forschungszentrum Jülich, 52425 Jülich, Germany

and

W. Speier

Institut für Chemie und Dynamik der Geosphäre (ICG), Forschungszentrum Jülich, 52425 Jülich, Germany

Received August 4, 1999; in revised form September 24, 1999; accepted October 11, 1999

The complex perovskite $BaCa_{(1+x)/3}Nb_{(2-x)/3}O_{3-x/2}$ (here $x = 0.18$), also referred to as BCN18, is a widely studied high-temperature proton conductor which has O-vacancies in the dry state accommodating highly mobile protonic defects in the wet state. Experimental evidence is given that BCN18 exposed to a very dilute acid (here HCl), or even hot water, undergoes a remarkable reaction to an amorphous state within a surface layer. The thickness of this layer ranges from tens of nm to several μm depending on exposure time. The amorphous layer is studied with TEM, XRD, XPS, SNMS, TRFA, and AFM. It is concluded that Ba and Ca are almost completely leached out of the surface layer. Protons penetrate into the solid, forming an intermediate, unstable solid acid, rich in Nb and O. The latter eventually collapses into an amorphous phase of Nb, O, and some water. A prerequisite of the above scheme inferred from the kinetics of the process is the presence of planar defects or channels of amorphous character in the initial BCN18 structure that allow rapid diffusion of Ba, Ca, and H. The present model assumes a block arrangement for the initial BCN18 with perfect perovskite structure inside the blocks, separated by thin amorphous slabs. © 2000 Academic Press

Key Words: **perovskites; amorphous phases; leaching; XPS; SNMS; TEM; AFM.**

1. INTRODUCTION

The perovskite-type structure offers a wide range of possibilities for modifying its chemical composition, such as doping or substitution, in either a disordered or an ordered manner. This gives us the opportunity to specifically design interesting material properties. A case in point is the potential application of perovskites as high-temperature proton conductors. Standard ternary perovskites are known to show proton transport when doped with a high concentration of acceptors. The uptake of protons is then generally considered to take place via the dissociative absorption of water by the lattice containing oxide ion vacancies charge compensating the acceptor dopant. In this respect, the wide class of mixed perovskites has attracted considerable interest since oxygen vacancies can be easily introduced by simply changing the stoichiometry. Indeed, mixed perovskites of type $A^{2+}B^{2+}_{1/3}C^{5+}_{2/3}O_3$, introduced by Nowick *et al.* (1–4), have been shown to act as "serious contenders" (1) in the search for fast high-temperature conductors suitable as electrolytes for a SOFC based on proton conduction, or as an electrolyte for humidity and hydrogen sensors. In particular, $BaCa_{(1+x)/3}Nb_{(2-x)/3}O_{3-x/2}$, with $x = 0.18$ (referred to as BCN18) has been identified as a model substance for the investigation of some of the more important features of high-temperature proton conduction (1–10). Introduction of the divalent Ca, generally considered to be positioned on every second NbO_2-layer, introduces a very high

[1]To whom correspondence should be addressed. Fax: 49-2461-612550. E-mail: T.Schober@fz-juelich.de.

0022-4596/00 $35.00
Copyright © 2000 by Academic Press
All rights of reproduction in any form reserved.

concentration of oxygen vacancies in the dry state, which may be filled according to

$$(H_2O)_{gas} + V_O^{\bullet\bullet} + O_O^x \Leftrightarrow 2OH_O^{\bullet} \quad [1]$$

(where the symbols have their usual meanings), leading to a protonated ceramic. Standard perovskite of the ABO_3-type containing divalent alkaline earth metal are known to be thermodynamically unstable in natural water near room temperature due to preferential loss of A cations in the AO sublattice (11). This then raises the question as to what extent a mixed perovskite such as BCN18 is affected by the presence of aqueous media and as to whether the BO_2 sublattice possibly stabilizes the substituted alkaline earth metal, here Ca.

In this paper we give evidence that BCN18 shows massive loss of alkaline earth ions as an effect of the reaction with aqueous media, as well as in dilute acidic solutions. Even more, structural changes leading to amorphization are observed in both cases. For our analysis we combined X-ray diffraction analysis, metallography, and total reflection fluorescence analysis (TRFA) with analytical techniques on the nanoscale, such as transmission electron microscopy (TEM), atomic force microscopy (AFM), and sputtered neutral mass spectrometry (SNMS). The electronic structure of the original material and the generated structures were investigated using X-ray photoelectron spectroscopy (XPS) and electron energy loss spectroscopy (EELS). Finally, we propose a model of the initial structure and the induced changes in the material.

2. EXPERIMENTAL

Synthesis of BCN18 was carried out long conventional lines from oxides and carbonates (4, 5). In most cases, the samples were sintered for 24 h at 1600°C. Most commonly, polycrystalline plates with a grain size of a few μm were used. Where needed, powder was prepared from such plates with a particle size of 1–2 μm. In a few cases, small single crystals were employed, grown by a special microwave technique (12). The acidic solution used was typically 0.3% HCl, if not indicated otherwise; for the SNMS measurement we used a 0.2% DCl in D_2O solution for which a pH of 0.9 was measured.

3. RESULTS

3.1. X-Ray Diffraction and TEM Results

X-ray diffraction. For the X-ray reference measurements, powdered BCN18 with a grain size of 1–2 μm was first dried in vacuum (10^{-6} Torr) at 600°C for 12 h. In Fig. 1 the raw X-ray diffraction data without background subtraction are shown—details are in the figure caption. The reflections found are in agreement with (9, 10), where a "dry" fcc lattice parameter of (0.84031 ± 0.000042) nm was reported. Due to ordering effects of the B-type atoms, the unit cell dimensions are doubled. Estimating the contribution of the amorphous background yields values between 10 and 20%. A short exposure, for 3 min, to a 5% HCl solution at room temperature produced marked changes in the diffraction pattern, notably an increase of the amorphous background. The intensity of the reflections decreased while the positions remained virtually unchanged. The same held true as an effect of the treatment in an aqueous solution, though much longer exposure times had to be applied. Figure 1 (right-hand inset) depicts the decreased intensity of the (220) reflection for the three cases discussed in the figure. Powder specimens treated for several hours in 5% HCl did not display any crystalline lines, only the amorphous background.

TEM. Evidence for a complete amorphization of very thin samples was obtained by TEM and electron diffraction (Figs. 2a and 2b). When thinned BCN18 TEM samples were exposed for 30 s to only a 0.3% HCl solution the former crystalline areas were totally converted to the amorphous phase (Fig. 2a). This occurred without cracks or mechanical disintegration to powder. Essentially, the shape of the affected area was maintained during the transition. The corresponding SAD patterns (Fig. 2b) displayed only two very broad rings typical of the amorphous state. Exposures for a few seconds only produced a two-phase situation in the sample, where rather round amorphous areas were embedded in the crystalline grains. We note that in TEM samples only about 50-nm-thick layers on each side have to be rendered amorphous (which is accomplished in ~30 s) while for X-ray diffraction effects several μm in depth have to be affected.

A similar effect is seen in the X-ray powder diffraction pattern of BCN18 after exposure to boiling water for 1 h. It displays amorphization effects similar to those in dilute acids.

3.2. Metallography

Exposing small chip with only several very large grains to a 0.6% HCl solution at 60°C for 2 min resulted in the formation of a thick surface layer of the amorphous phase. This layer became locally detached or delaminated from the matrix as seen in Fig. 3. The fringes visible in Fig. 3 are interference effects produced by the gap between the amorphous layer and the matrix where delamination occurred, presumably as a consequence of high mechanical stress.

3.3. SNMS, XPS, and TRFA Measurements of Stoichiometric and Amorphous Samples

SNMS measurements were carried out in a SIMSLAB410 (Fisons) unit using an O_2^+ ion source. The sputtering rate

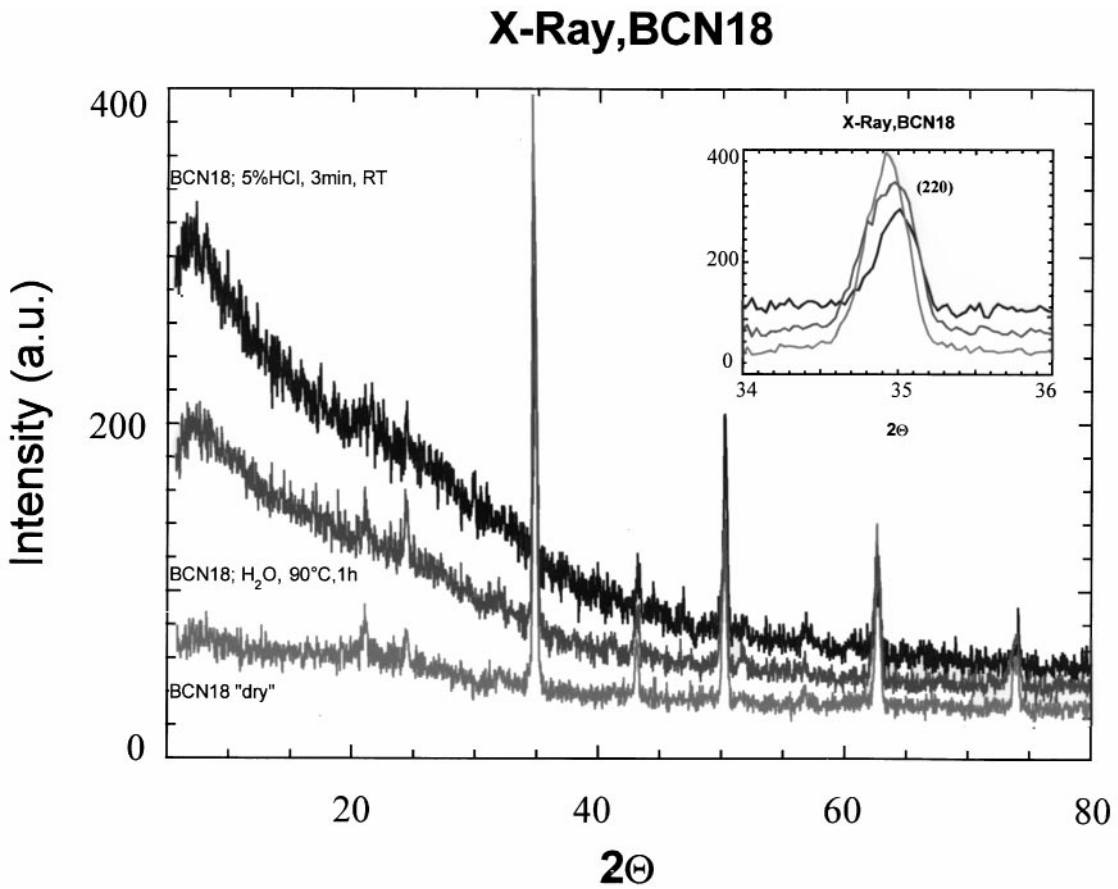

FIG. 1. X-ray powder diffraction data of BCN18, no background correction. Lowest curve, untreated, dry BCN18 powder; center curve, BCN18 powder treated for 1 h in 90°C hot water; upper curve, BCN18 powder treated in 5% HCl for 3 min at R.T.

was determined by profilometry of the sputter crater. The concentration profiles of the different components of the stoichiometric sample reach plateau values after about 20 nm, indicative of a constant sputtering rate for all matrix elements (Fig. 4a). Due to the well-known elevated efficiency for alkali and alkaline earth elements, the Ca signal is higher than that of Nb although BCN18 has a lower Ca content. The depth profile of the short leach experiment (3 min in 5% DCl) clearly shows that Ba and Ca are selectively removed from a surface layer roughly 100–120 nm deep (Fig. 4b). TRFA analysis of the products in HCl confirms that essentially only Ba and Ca are found in the solution. The ratio of Nb to Ba in the solution is of the order of 10^{-5}. This is in agreement with the almost unchanged depth profile of the Nb concentration. The long exposure (20 h) to the dilute HCl solution leads to qualitatively similar effects (Fig. 4c). The intensity for Ba and Ca is reduced in a layer extending to more than 3 μm in depth by over two orders of magnitude. The Nb level remains practically unchanged with depth.

The SNMS and TRFA data definitely establish a link between the amorphization and the Ba and Ca depletion in the surface layer leading to a change in the chemical composition. We therefore expect chemical shifts in X-ray core peaks of the constituents of BCN18. The XPS data were gathered for a reference sample and for one with an amorphous surface layer in a Leybold spectrometer with a monochromator calibrated using standard techniques. As reference, the binding energy of the C 1*s* level (284.6 eV) was used. We note that the surface of *ex situ* prepared samples is always contaminated with carbon compounds.

XPS of stoichiometric BCN18. The alkaline earth XPS spectra of the stoichiometric samples showed that the Ba 3*d* core line consists of only one component (Fig. 5a). In Table 1, all the binding energies and FWHM values for all constituents of BCN18 are listed, for both the stoichiometric and the amorphous case. The Ca component can only be fitted with two doublets as shown by the spectrum Ca 2*p* (Fig. 6). The fit routine used was PeakFit (16). The chemical

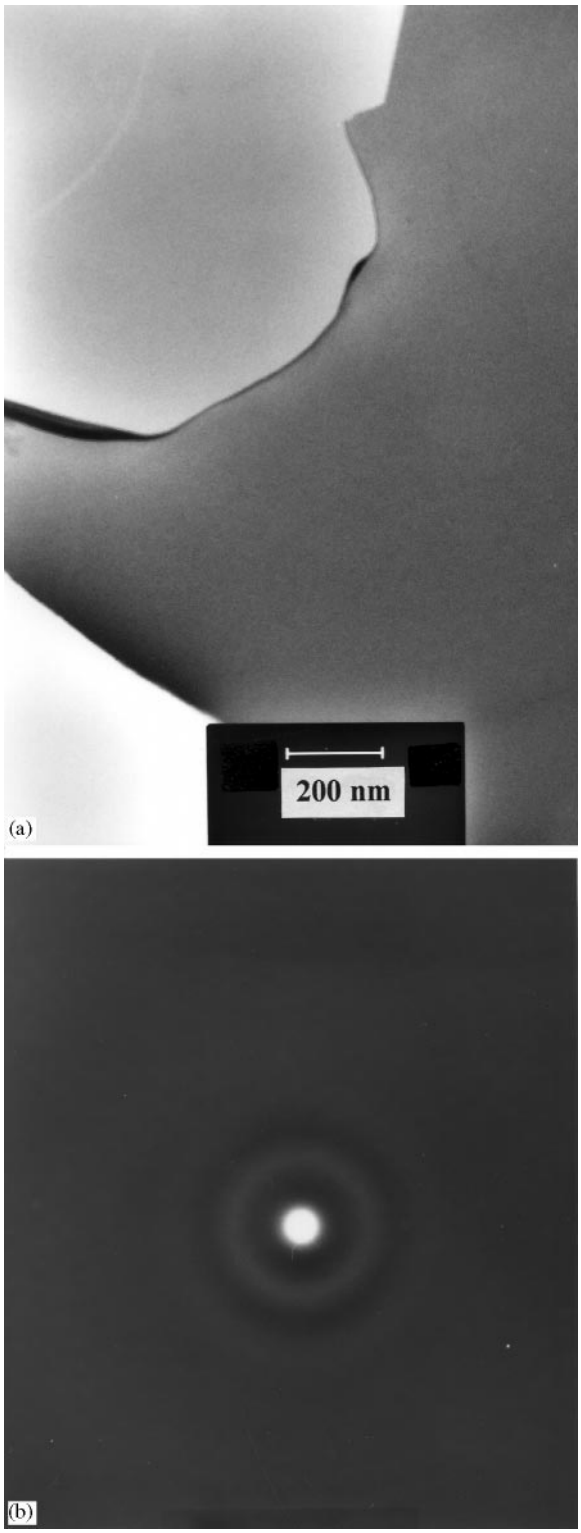

FIG. 2. TEM micrographs of locally electron-transparent BCN18 samples exposed to 0.2% HCl at R.T. for 30 s. (a) (Bright field) Previously crystalline area displaying extinction contours converted to the amorphous phase with totally uniform background intensity. The overall shape of the crystalline area was preserved during the transformation without crack formation. (b) SAD pattern of the region shown in (a) *after* acid exposure. The pattern is typical of the amorphous, glassy state.

shift for the second form of Ca amounted to 1.8 eV. To fit the core line of Nb (3d), several doublets had to be used too (Fig. 7a). The three doublets were shifted by 0.8 and 1.5 eV, respectively. The O 1*s* line of an *ex situ* prepared sample contains additional components, arising from the absorption of carbon oxides, water, or hydroxyl groups on the surface, which are mixed with the original oxygen line of BCN18.

XPS of the amorphous phase. The most spectacular change in the XPS surface spectra was the disappearance of the Ca coreline. The Ba 3*d* core line has now, in contrast to the initially crystalline sample, two components displaced by 1.1 eV (Fig. 5b). The major component Nb 3*d* core line is located at a binding energy of 205.3 eV. A small

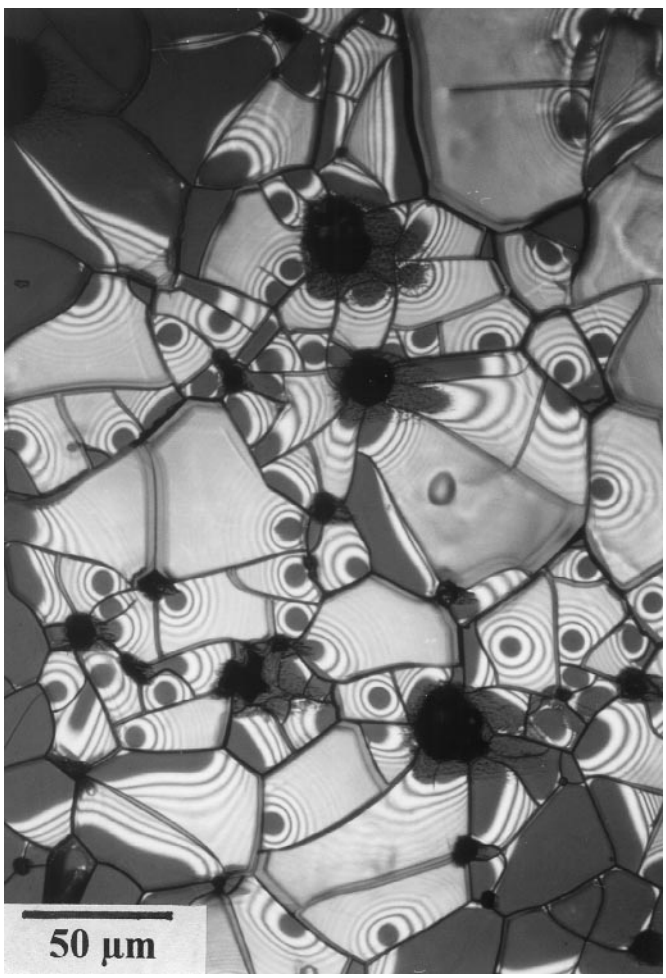

FIG. 3. Optical micrograph of a polycrystalline piece of BCN18 exposed for 2 min at 60°C to a 0.6% HCl solution. (White areas) Here the thick amorphous layer became locally detached from the crystalline matrix due to mechanical coherency stresses as witnessed by the interference fringes arising due to the gap between the two layers. (Dark areas) Here there is still satisfactory bonding between the amorphous overlayer and the crystalline matrix.

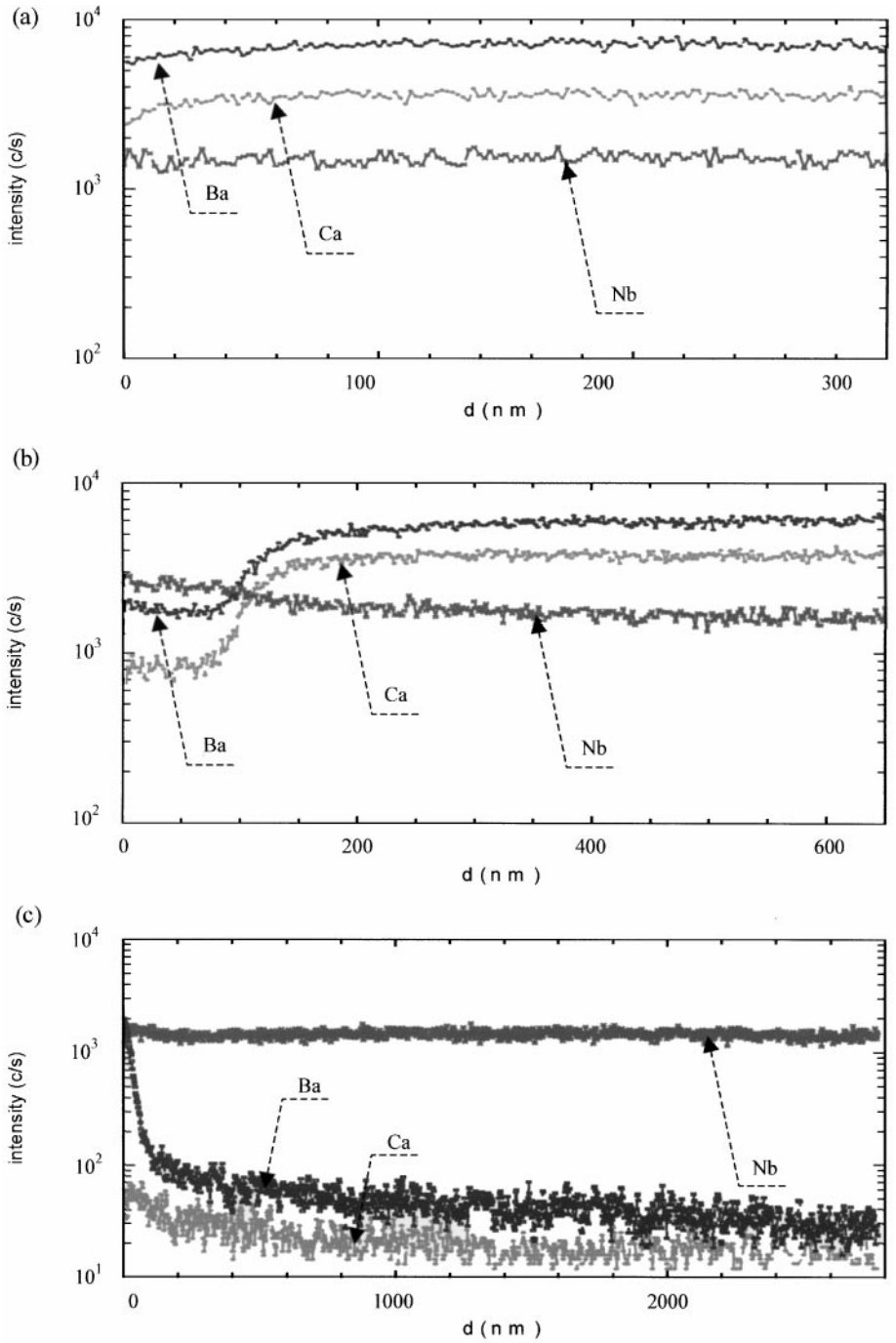

FIG. 4. SNMS depth profiles of Ba, Ca, Nb, and O. (a) Untreated, stoichiometric BCN18 sample, after a few monolayers constant intensity levels were observed for the four elements. (b) BCN18 sample leached for 3 min in a 5% DCl solution. Ba and Ca are selectively removed to a depth of 100–120 nm while Nb and O remain approximately constant. (c) BCN18 sample leached for 20 h in a 5% DCl solution. Note massive depletion of Ba and Ca extending to over 3 μm in depth with no apparent change in the Nb and O signals.

contribution to the Nb 3*d* XPS spectrum is provided by Nb with a higher valence at a binding energy of 206.1 eV (Fig. 7b).

EELS analysis. The XPS data demonstrate that the Ca cations have different binding energies in stoichiometric BCN18. The exit depth of XPS (Al$K\alpha$) is of the order of several nm. The observed changes in the Ca core lines may be caused by surface artifacts. TEM provides the opportunity to record an electron loss spectrum at a much higher penetration depth (up to 50 nm). EELS spectra of the L_{23}

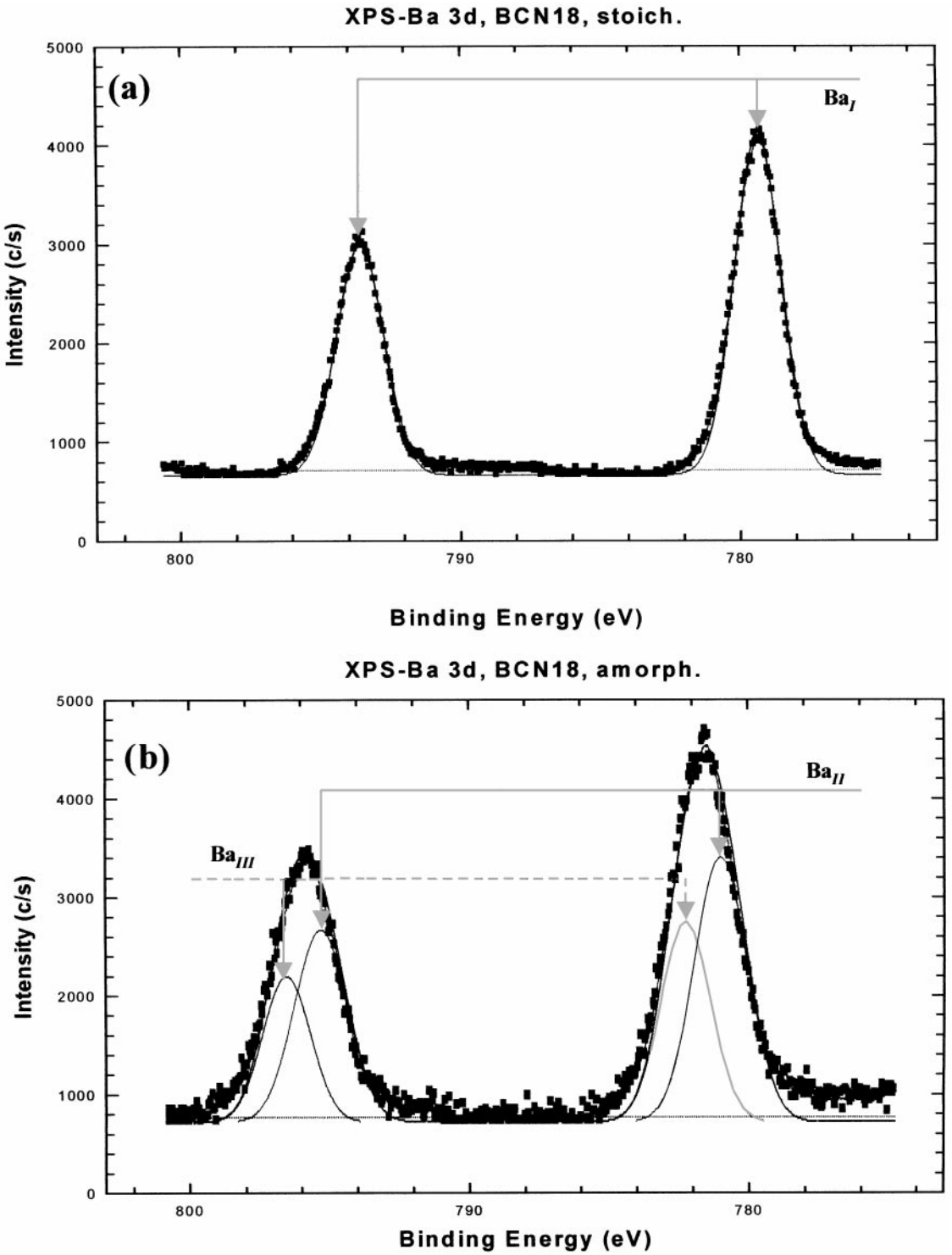

FIG. 5. XPS, Ba 3*d*. (a) Stoichiometric, untreated BCN18, only one Ba 3*d* doublet component is visible. (b) Amorphous BCN18 after surface leaching, two Ba 3*d* doublets are now visible.

edge (2*p*–3*d* transition) give a picture similar to that given by the XPS data. EELS for Ba show that the Ba cations exist at, or near, the surface only in one chemical form (Fig. 8a). On the other hand, EELS for Ca suggest that we are dealing with two kinds of Ca cations in the matrix (Fig. 8b) since fitting the measured spectrum with two reference spectra for $CaCO_3$ displaced slightly in energy gave a reasonable overall agreement.

TABLE 1
Binding Energy (B.E.) (eV) of Ba 3*d*, Ca 2*p*, Nb 3*d*, C 1*s* Core Lines of Stoichiometric BCN18 (A) and Amorphous BCN18 (B) in Comparison with Literature Data for Reference Compounds

		Ba $3d_{5/2}$	Ba $3d_{3/2}$	Ba $3d_{5/2}$	Ba $3d_{3/2}$	Ba $3d_{5/2}$	Ba $3d_{3/2}$	Ca $2p_{3/2}$	Ca $2p_{1/2}$	Ca $2p_{3/2}$	Ca $2p_{1/2}$	Nb $3d_{5/2}$	Nb $3d_{3/2}$	Nb $3d_{5/2}$	Nb $3d_{3/2}$	Nb $3d_{5/2}$	Nb $3d_{3/2}$	C 1*s*
		I	I	II	II	III	III	I	I	II	II	I	I	II	II	III	III	I
A	B.E.	779.3	794.5					344.1	347.9	346.1	349.7	205.4	208.2	206.2	209	206.9	209.9	284.6
B	B.E.			781	796.2	782.1	797.6					205.3	207.8	206.1	208.9			284.6
Literature		BaO		Ba		$Ba(OH)_2$		Ca		CaO		NbO		NbO_2		Nb_2O_5 (13)		207.5
		779.9 (13)		780.6 (13)		784.1 (14)		346.8 (13)		347.3 (13)		204.7 (13)		205.9 (13)		$BaNb_2O_6$ (13)		207.1
		779.6 (13)		779.3 (13)				346.3 (13)		346.7 (13)		203.7 (13)		Nb^{+4} in $KNbO_{3-x}$		$LiNbO_3$ (13)		207.1
		779.1 (13)						345.9 (13)		346.1 (13)		202.8 (13)		205.0 (15)		$CaNb_2O_6$ (13)		207.0
												Nb^{+2} in $KNbO_{3-x}$				$Ca_2Nb_2O_7$ (13)		206.9
												203.8 (15)				$KNbO_3$ (15)		206.9
																$KNbO_3$ (13)		206.5

3.4. AFM Study of the Surfaces of Stoichiometric and Amorphous Samples

Atomic force microscopy (AFM) is well suited for surface topography studies of nonconducting solids. The present transition crystalline stoichiometric phase → amorphous phase should also lead to marked changes in the surface topography. The AFM measurements were performed in the tapping mode in an AFM instrument (Nanoscope, Digital Instruments) with a built-in x–y table and CCD camera, providing the ability to relocate and scan the same area after the amorphization. The traditional surface preparation procedure of polishing using liquids was not practical here due to the fast reaction of BCN18 with water and selective leaching of Ba and Ca. Surface preparation was therefore carried out by cleavage. Areas with optically flat facets were selected as reference surfaces (Fig. 9a). The surface roughness of such areas was only a few nm. AFM images of cleaved surface areas show a characteristic configuration of parallel stripes with distances of several tens of nm.

After a brief exposure to dilute HCl this characteristic pattern of parallel stripes was found again at the same positions as in the untreated sample (Fig. 9b). The width of the stripes remained unchanged while dramatic differences occurred in the topography between the stripes. Small variations in height of $\pm$ several Å on the surface of the stoichiometric sample turned into deep canyons after the HCl treatment. Preferential attack along the boundary between the stripes produced canyons a few hundred Å deep. Surface roughness increased by the factor $\sim 10^2$.

A more macroscopic view of the amorphization of an area is provided in Figs. 10a and 10b. An originally flat area (Fig. 10a) was converted to an island structure of the amorphous phase with deep canyons in between (Fig. 10b).

4. DISCUSSION

The conventional assumption about proton uptake of BCN18 at rather high temperatures is that this absorption is linked to the presence of a high concentration of oxygen vacancies in the dry state as described by Eq. [1]: $(H_2O)_{gas} + V_O^{\cdot\cdot} + O_O^x \Leftrightarrow 2OH_O^{\cdot}$. This reaction implies, however, that BCN18 is inert or resistant to H_2O. There is no participation of cations.

The present experimental facts obtained at much lower temperatures in aqueous media confront us with a very different picture, where the chemical composition and the crystal structure of BCN18 may undergo dramatic changes:

(1) The X-ray results definitely show that the same structural changes occur in BCN18 upon exposure to water or weak acids, although on different time scales. After HCl exposure the diffractograms show a faster increase of the background (which is a measure of the degree of

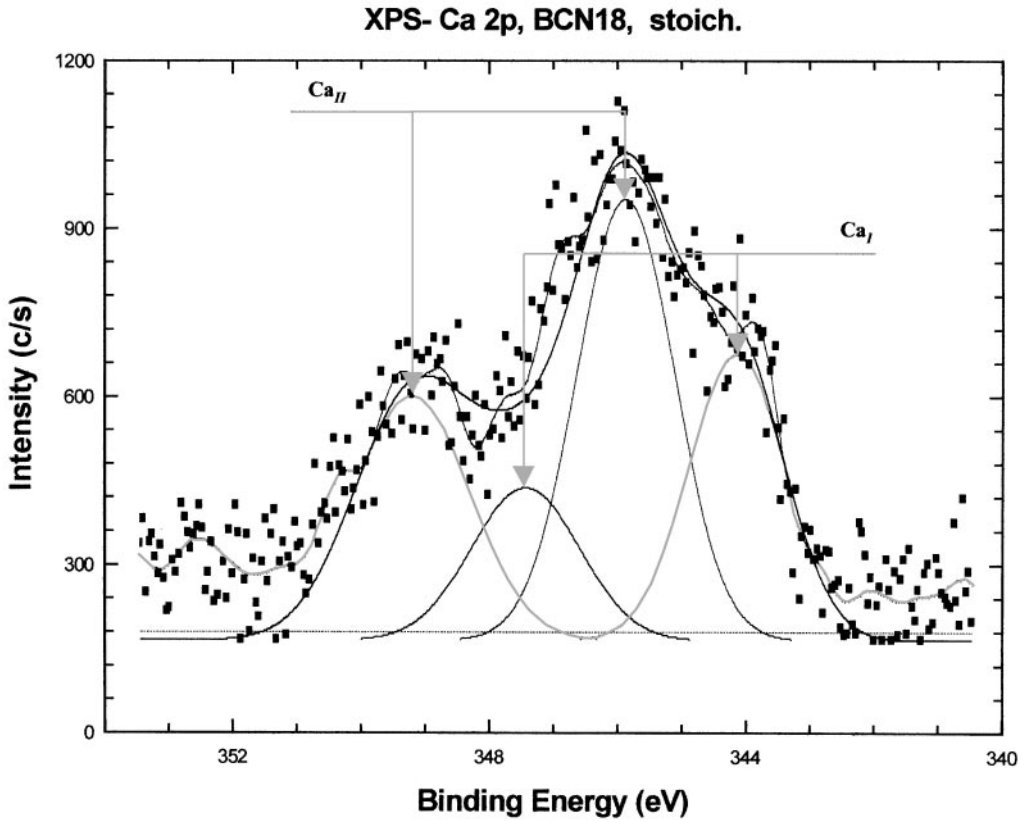

FIG. 6. XPS, Ca 2*p*, BCN18 stoichiometric, untreated. To fit the experimental spectrum at least two Ca doublets are required.

amorphization) than after water exposure, for identical exposure times. In both cases, the intensity of crystalline peaks decreases while the background intensity increases. The diffraction patterns of samples treated for long periods (>12 h) with water and those after short acid exposure (>30 s) do not exhibit reflections, indicative of amorphization within the full penetration depth of the X-rays.

(2) Amorphization is linked to the selective leaching of the cations Ba and Ca. Evidence stems from the SNMS concentration profiles of Ba and Ca and from the chemical analysis by TRFA of the elements in the solutions after leaching. The decreasing Ba and Ca concentrations in the surface layer of amorphous samples show that amorphization starts at the solid–liquid phase boundary. With time the amorphous–crystalline boundary is displaced in the direction of the bulk. In contrast to the concentrations of Ba and Ca, the Nb concentration remains almost constant. However, in the NbO_2 sublattice structural consequences of the amorphization manifest themselves: no crystalline Nb-rich phase is observed.

(3) The present phenomena are similar to the leaching effects observable in nature in ABO_3 minerals in water-containing environments (11), or to the cation exchange phenomena in ternary oxides such as $LiNbO_3$ (17). The differences lie in the crystal structures after leaching, which are crystalline for ABO_3 type perovskites while BCN18 becomes amorphous. The present amorphization and leaching processes can be described in analogy to previous leaching or cation exchange processes by the equations

$$\begin{aligned} &BaCaNb_2O_9 + 4H_2O\ (5H_2O) \\ &\quad \rightarrow 3Ba(OH)_2 + Ca(OH)_2 + Nb_2O_5\ (Nb_2O_5 \cdot H_2O) \\ &Ba_3CaNb_2O_9 + 8HCl \\ &\quad \rightarrow 3BaCl_2 + CaCl_2 + 2HNbO_3 + 3H_2O \\ &BaCl_2 + CaCl_2 + H_2O \\ &\quad \rightarrow Ba(OH)_2 + Ca(OH)_2 + 2Cl_2\uparrow, \end{aligned} \qquad [2]$$

where the Cl_2 obviously would be unstable in water for $HClO_3$ and HCl formation. Evidence for the chemical route leading from an intermediate unstable solid acid to $Nb_2O_5 \cdot H_2O$ or $HNbO_3$ compounds comes from the observed thermal desorption of water. These compounds are

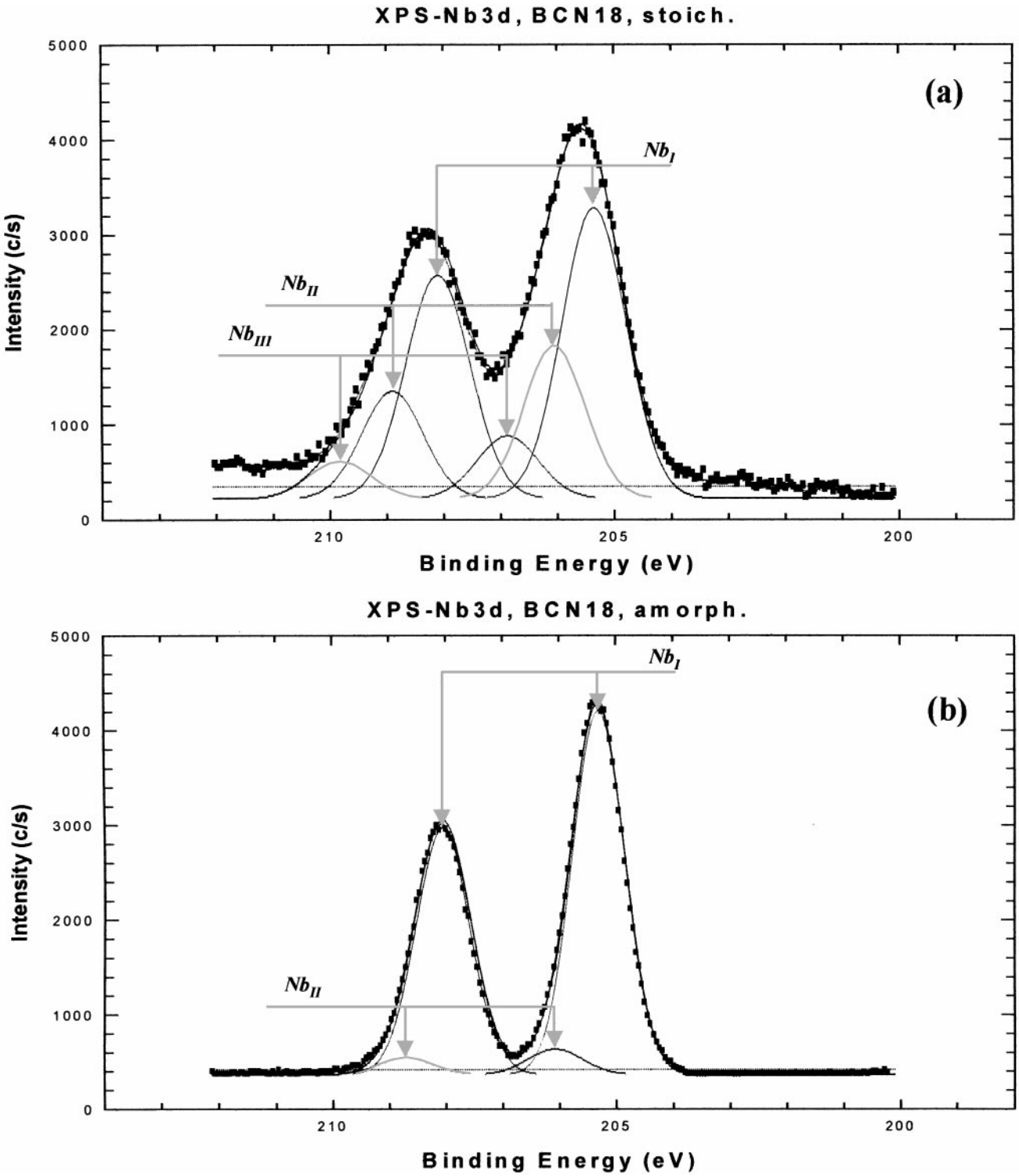

FIG. 7. XPS Nb 3*d*, BCN18. (a) Stoichiometric, untreated compound. At least three Nb 3*d* doublets are required to describe the observed spectrum. (b) After surface amorphization by leaching. Two Nb 3*d* doublets describe the experimental spectrum.

unstable thermally, giving rise to the net production of Nb oxide and water.

In contrast to the reactions in standard ABO_3 crystals with the selective removal of *A* cations in *A*O sublattices, the amorphization rate of BCN18 is surprisingly high and increased by two or three orders of magnitude. These differences are associated with the structure of the ceramic and the consequences in the electronic structure.

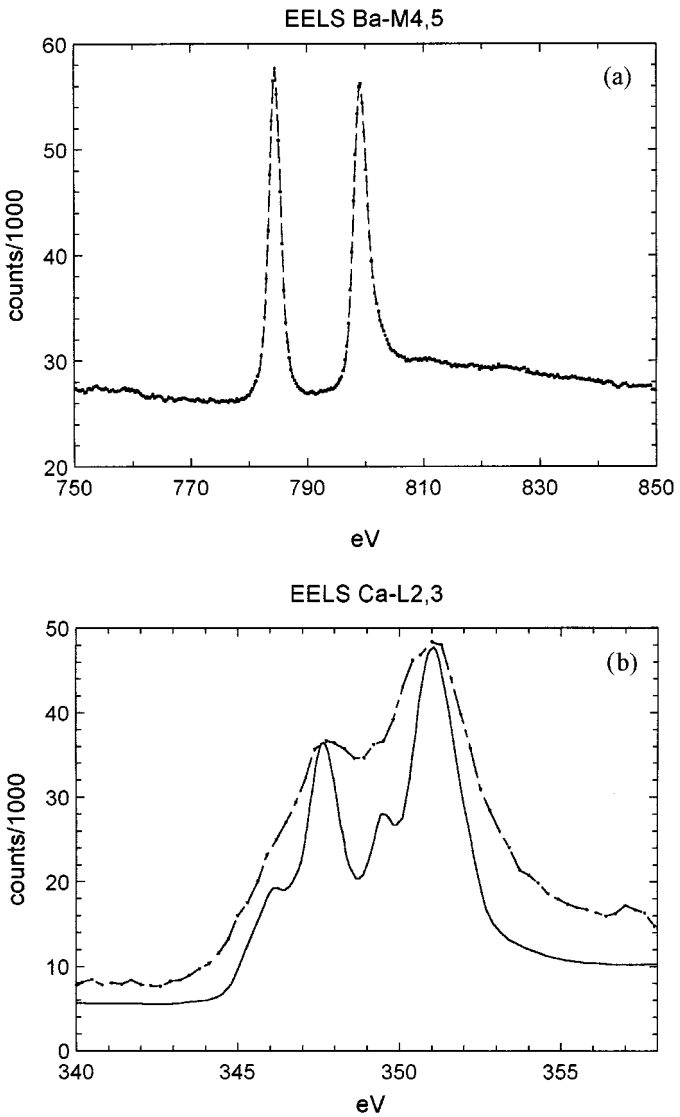

FIG. 8. EELS spectra of untreated stoichiometric BCN18. (a) Ba M 4, 5. (b) Ca L 2, 3. (Full line) Literature reference spectrum. (Dashed curve) Present BCN18 sample.

The fast penetration of constituents of liquid media, such as protons, into BCN18 may be explained by the existence of planar, stacking fault-like defects from which we explicitly exclude normal grain boundaries. These kinds of extended defects which intersect the surface of a facet of a crystal are clearly visible in the AFM pictures. The preferential dissolution in weak acids parallel to such defects shows AFM images of the same facets (Fig. 9b). Tracer diffusion experiments with ^{18}O in single crystals of $KNbO_3$ have proved that the diffusivity parallel to such defects is 4 to 6 orders of magnitude larger than the classical random-walk diffusivity (18). There is ample evidence that the Nb oxides have a more complex system of extended defects than the titanates (19). The extended Wadsley defects, which may cause the formation of Magneli phases in Ti oxides, may intersect in the case of niobates along three equivalent directions. The later effect may lead to the formation of a block structure [19]. TEM SAD images of particles produced by grinding of the ceramic display complicated diffraction effects, which may also be indicative of the existence of such a nanoblock structure. We note that $SrTiO_3$ nanocrystals prepared in the same way display well-defined single-crystal patterns. This excludes mechanical grinding as the possible reason for the formation of a nanoblock structure in BCN18. In BCN18 the separation between the different blocks is not on an atomic scale as in the antiphase boundary [19]. Instead, our data suggest that one is dealing with a thin amorphous slab separating the blocks.

The complicated structure of BCN18 manifests itself in the electronic structure as evident by the XPS data. The simple picture of a single ion valence per ion (Ba^{2+}, Ca^{2+}, Nb^{5+}) is in this material presumably only valid for the Ba cations. The Ba 3*d* core line exhibits only one doublet which corresponds to the one in BaO (779.6 eV) (see Table 1). On the other hand, three possible chemical forms may be assigned to the Nb cations (Table 1). The component with the highest binding energy (B.E.) (Nb_{III}: 206.9 eV) has a B.E. similar to that of Nb in $KNbO_3$. Classically interpreted, this component is ascribed to cations with a nominal valence of $+5$. This component contributed about 15–20% to the concentration of all Nb cations. The second doublet Nb 3*d* (Nb_{II}) is shifted by 0.7 eV to lower B.E. and originates from tetravalent Nb cations (similar to NbO_2). Roughly 25% of the Nb is in this electronic state. The largest contribution to the Nb core line ($>60\%$) stems from Nb ions with even smaller B.E. (Nb_I). Literature data suggest that the valence is in the range $+2$ to $+4$ with reference to NbO and NbO_2, respectively (see Table 1). On the basis of our current understanding, several factors may contribute to the observed variance in core level, namely, the substituted Ca on octahedral sites, the in-built oxygen vacancies, and the character of the amorphous phase already present in the original material. We are not able to correlate unambiguously the three core levels to the different contributing factors. We assign the core level with highest binding energy (Nb_{III}) to an otherwise undisturbed NbO_2-layer (with a nominal valence of $+5$). The other doublets (Nb_{II}, Nb_I) have to be taken as a signature of a change in valence due to the substitution of divalent Ca and incorporation of oxygen vacancies within the NbO_2 sublattice. Large variations in valence as a consequence of the incorporation of oxygen vacancies are not surprising (15). Surprisingly, the core level with the lowest binding energy (and lowest valence, Nb_I) shows the highest intensity prior to treatment and thus may be attributed to the main crystalline component of the starting material, indicative of a local composition in the form of NbO_{2-x}. But, the assignment may be further

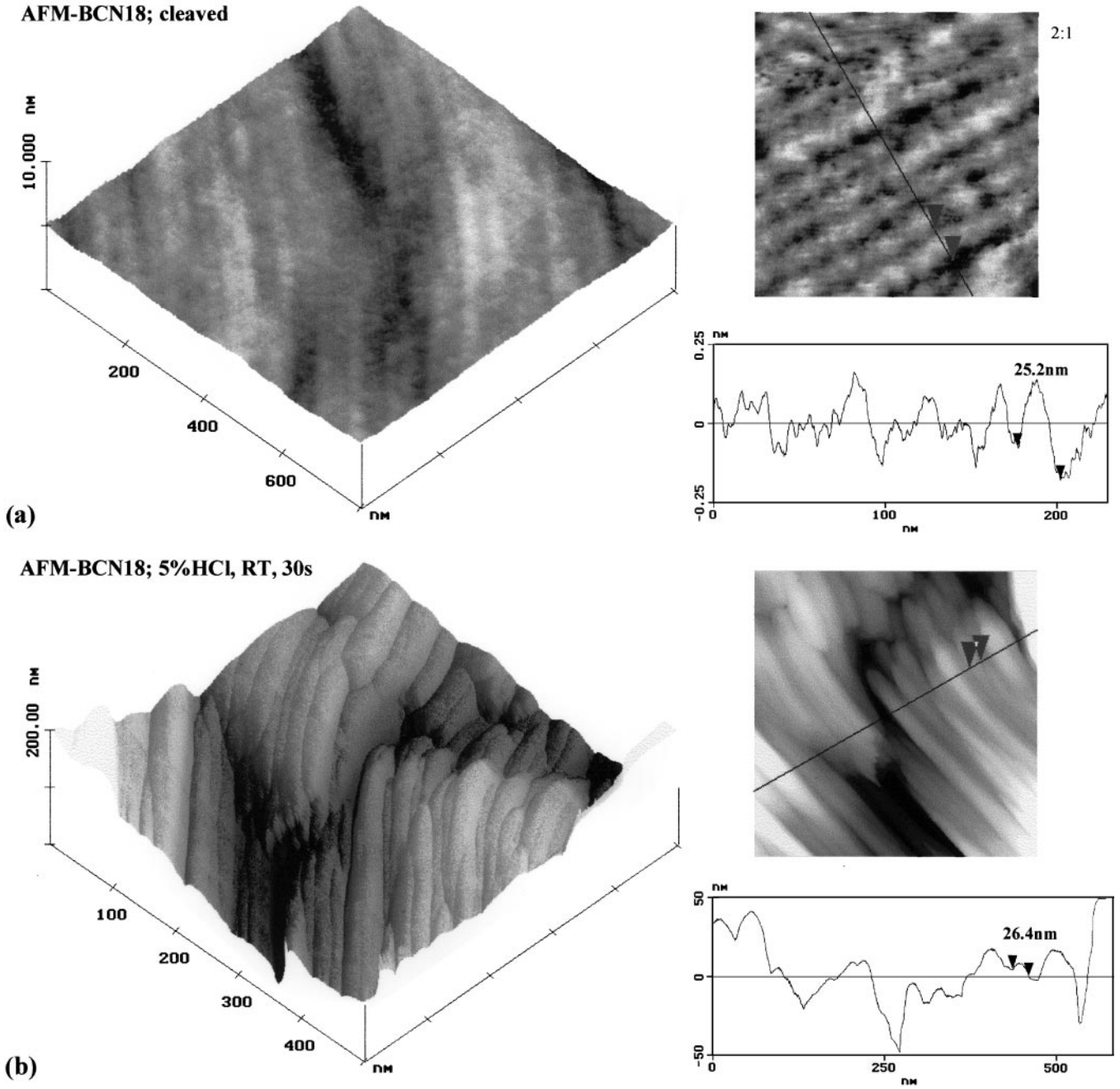

FIG. 9. AFM micrograph of BCN18 surface. (a) (Left-hand side) as cleaved, flat segment. (Right-hand side) Scan of surface along line. Layer structure is visible. (b) Same area after exposure to 5% HCl at R.T. for 30 s. A deep canyon system has evolved due to preferential dissolution of matter between the blocks of the block structure. (Right-hand side) Line scan to show the depth of the canyon structure.

complicated by the fact that the measured surfaces were been prepared *ex situ* and thus influenced the spectral distribution as a result of contact with the humidity always present in air. Interestingly, the spectrum after complete amorphization within the surface layer (compare with Fig. 7b) is almost completely dominated by this core level. Anyway, a large spectrum of Nb valences in the surface prior to treatment signifies that the electroneutrality of such compounds can be established by a change in valence. This may be at variance with the interpretation of the dominant role of oxygen vacancies as charge-compensating elements. This was also seen in the amphoteric properties of 3*d* or 4*d*

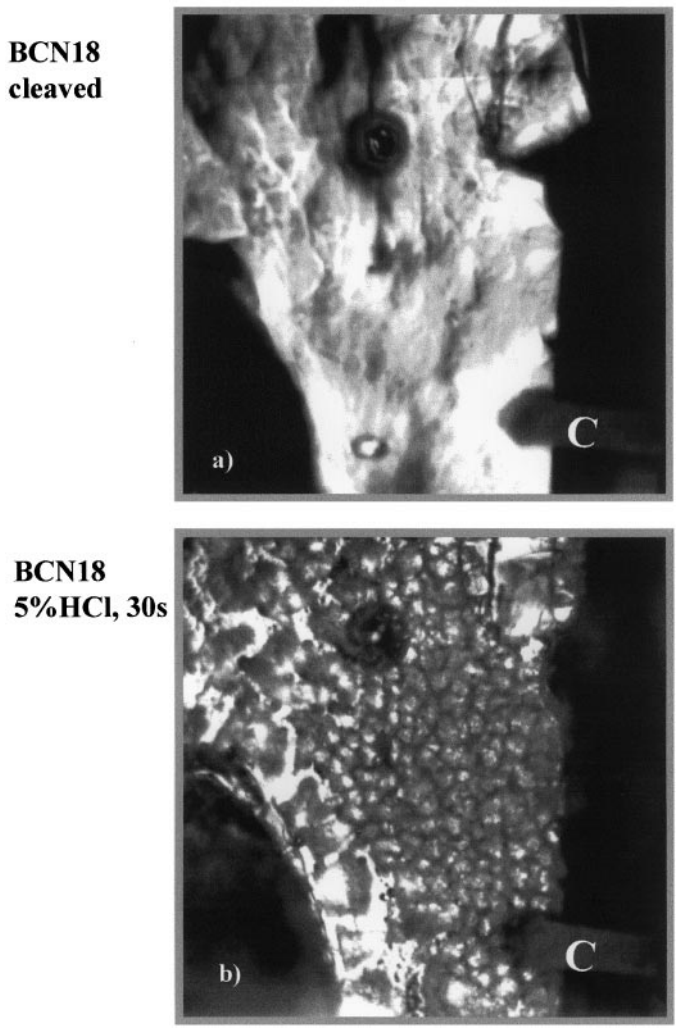

FIG. 10. AFM micrograph of BCN18 surface. (a) Cleaved surface, untreated, with fiducial marks. (b) Same area shown in (a) after 30 s exposure to 5% HCl. New surface topology consists of islands of the amorphous phase separated by deep canyons.

transition metal ions and was shown and discussed for other niobates (e.g., $KNbO_3$ (18)).

The ion valences based on XPS are here interpreted in a classical manner (integer valences). This is not an acceptance of such ionicities in perovskites in view of the large covalent character. It is a compromise in the light of a missing consensus in the works on the theoretical determination of the covalent contribution. In fact, in the prototypical perovskite $BaTiO_3$ the valence is not indicated as nominally $+4$; depending on the calculations, it varies between $+3.18$ and $+0.19$ (20). The same holds for the niobates. Even a charge of $+0.63$ has been reported for Nb (21) in lieu of the nominal static charge of $+5$.

The core-level spectra of Ca cannot be interpreted in a straightforward manner, partly due to the ambiguities in the values reported in the literature for the core levels of Ca metal and CaO (see Table 1). There is evidence, from both XPS and EELS, that Ca has to be considered present in the original material in two different local chemical surroundings. The core level with the highest binding energy (Ca_{II} in Fig. 6) is energetically positioned in between Ca metal and CaO (Table 1). We point out that the second component (Ca_I) is situated even somewhat below the B.E. of the metallic state. This shift is unexpected, indicating that Ca must be in chemical surroundings which favor some trend toward an anionic character (in this context, note that K in stoichiometric $KNbO_3$ was assigned the valence -0.87 in (21) or toward a potentials barriers effect leading to a local band bending. This peak may then be tentatively attributed to the existence of the amorphous phase in the starting material and may be correlated with the low core-level binding energy (or low valence) of Nb.

The analysis of the electronic structure of the amorphous surface layer of BCN18 after exposure to weak acids confirms the SNMS results on the selective leaching of alkaline earth cations. The strongest Ca line (here Ca 2*p*) cannot be detected by XPS after leaching. Yet, one can still distinguish two different doublets of Ba 3*d*. The B.E. of both components of the Ba 3*d* line have shifted by 0.6 (Ba_{II}) and 1.7 eV (Ba_{III}) with respect to the original core level. This signifies that the B.E. of the first doublet may correspond to metallic Ba (Ba_{II}, see Table 1). The anomalous position of the second doublet may be explained by the influence of local barriers as mentioned for the untreated surface or the formation of $Ba(OH)_2$ (see Table 1). As already mentioned, the analysis of the XPS Nb core line after treatment is dominated by only a single component (almost completely Nb_{III}), attributing a valence between $+2$ and $+4$ or a composition in the form of NbO_{2-x} to the amorphous lattice.

In Figs. 11a and 11b, a schematic model of the block structure and leaching phenomena is presented. Untreated BCN18 is viewed to consist of blocks of the perfect, crystalline phase separated by very thin slabs of a presumably amorphous phase enriched in Ca with respect to Ba. In standard X-ray or neutron diffraction, only the diffraction peaks of the crystalline phase are visible. The frequently neglected background stems, however, from the above amorphous slabs. When the left-hand side of the sample is exposed to a weak acid (Fig. 11a) Ba and Ca go into the solution along the original channel system. The BCN18 blocks decrease in size due to the formation of an amorphous Nb-rich oxide layer around them. In an atomic level it is seen that protons enter the structure. Ba and Ca leave their regular positions to the left of the white, dashed reference line and leave behind Nb–O octahedra containing some water, which eventually collapse into the disordered, amorphous phase.

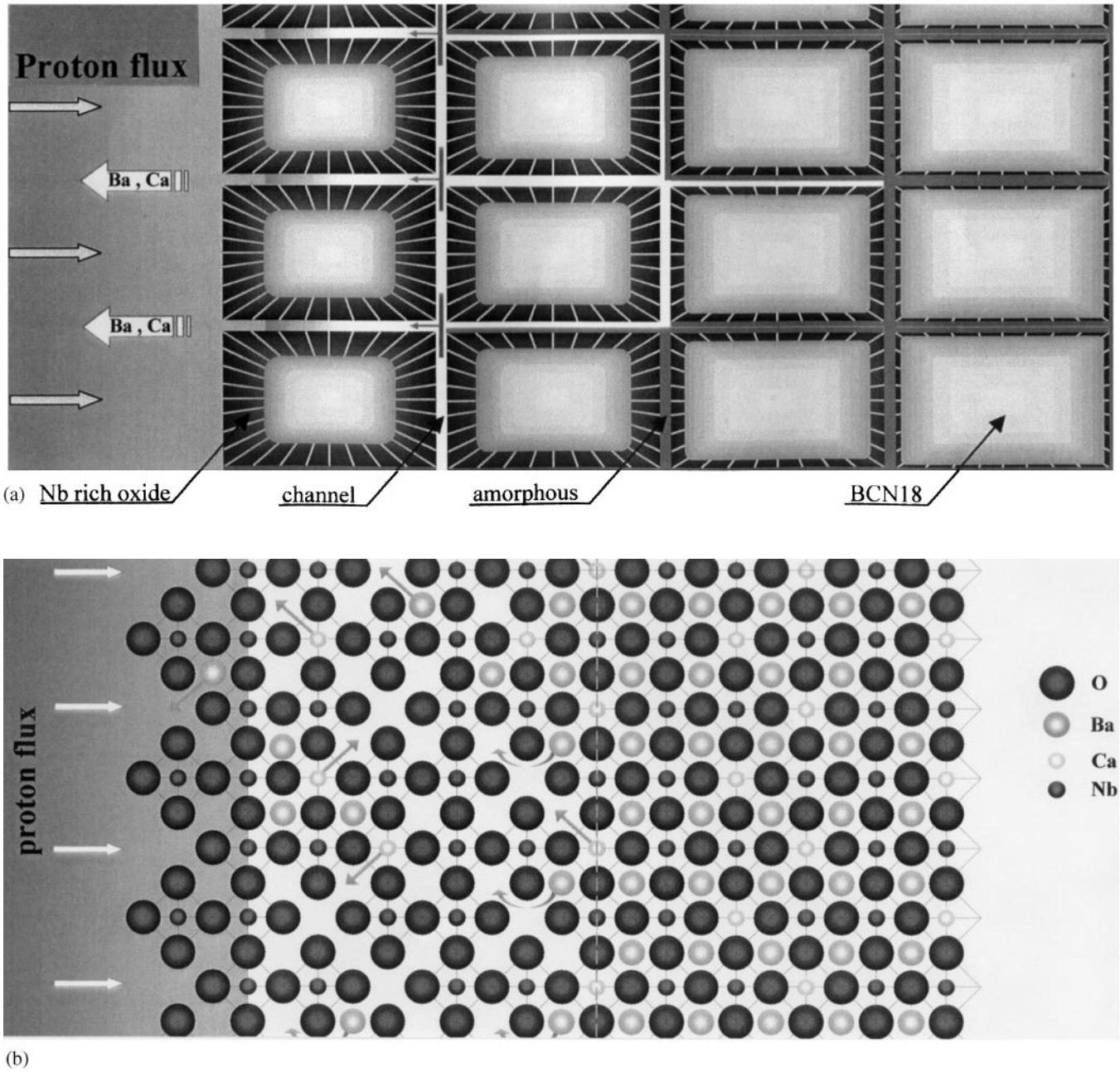

FIG. 11. Model of the leaching phenomena occurring in BCN18 when exposed to dilute HCl. (a) Mesoscopic model. (Right-hand side) Untreated BCN18 consists of blocks of the perfect crystalline BCN18 phase separated by very thin slabs of a presumably amorphous Ca-rich phase. When dilute acid is offered from the left-hand side, Ba and Ca go into the solution following the original channel system. Protons enter the sample along the channel system. Original crystalline BCN18 blocks decrease in size due to the formation of an amorphous Nb-rich oxide ($H_2O * NbO_{2-x}$) layer around them. (b) Microscopic model. To the right of the vertical dashed line the projected original BCN18 structure is seen. If dilute acid is present at the left side, protons rush into the solid and produce cation exchange processes. Ba and Ca leave the sample. Eventually, the surface layer consists of unstable Nb–O octahedra which collapse into an amorphous phase.

5. CONCLUSIONS

The presented results confirm the well-known phenomenon of the leaching of simple perovskites for a mixed perovskite such as BCN18. Moreover, Ca on *B*-positions is leached in the same way as Ba on *A*-positions. This indicates that both *A*- and *B*-ions, as long as they are alkaline earth, are subject to cation exchange. Our observations point to extremely fast leaching kinetics, probably due to a block structure of the parent phase. In contrast to in simple

perovskites, where the boundary between the *A*-ion-leached regions and the parent phase is crystallographically sharp and the product phase is crystalline (22), leaching in the present complex perovskites produces an amorphous phase with a diffuse interface. The experimental data thus give evidence that a mixed perovskite such as BCN18 has to be considered thermodynamically unstable in aqueous media at low temperatures, with a loss of material and subsequent structural changes. Finally, the present XPS results shed new light on the classical picture of O-vacancies maintaining electroneutrality in this kind of material. Possibly, electroneutrality is achieved here in part by valence changes.

REFERENCES

1. K. C. Liang, Yang Du, and A. S. Nowick, *Solid State Ionics* **69,** 117–120 (1994).
2. A. S. Nowick and Yang Du, *Solid State Ionics* **77,** 137–146 (1995).
3. Yang Du and A. S. Nowick, *Mater. Res. Soc. Symp.* **369,** 289–294 (1995).
4. Yang Du and A. S. Nowick, *Solid State Ionics* **91,** 85–91 (1996).
5. T. Schober, J. Friedrich, D. Triefenbach, and F. Tietz, *Solid State Ionics* **100,** 173–181 (1997).
6. F. Krug and T. Schober, *Solid State Ionics* **92,** 297–302 (1996).
7. H. G. Bohn, T. Schober, T. Mono, and W. Schilling, *Solid State Ionics* **117,** 219–228 (1999).
8. T. Schober, H. G. Bohn, T. Mono, and W. Schilling, *Solid State Ionics* **118,** 173–178 (1999).
9. T. Mono and T. Schober, *Solid State Ionics* **91,** 155–159 (1996).
10. T. Mono, Ph.D. Thesis, University of Aachen, 1997.
11. H. W. Nesbitt, G. M. Bancroft, W. S. Fyfe, S. N. Karkhanis, A. Nishijima, and S. Shin, *Nature* **289,** 358 (1981).
12. M. Barton, to be published.
13. John F. Moulder, William F. Stickle, Peter E. Sobol, and Kenneth D. Bomben, "Handbook of X-Ray Photoelectron Spectroscopy—Physical Electronics" (J. Chastain, Ed.), Perkin-Elmer, Eden Prairie, MN, 1992. [And quoted references]
14. E. Langenscheidt, private communication, FZ Jülich.
15. K. Szot, W. Speier, and W. Eberhardt, *Appl. Phys. Lett.* **60,** 1190 (1992).
16. PeakFit 4.0, SPSS, Science Software (http://www.spss.com).
17. J. L. Fourqet, M. F. Renou, R. De Pape, H. Theveneau, P. P. Man, O. Lucas, and J. Panneter, *Solid State Ionics* **9&10,** 1011–11014 (1983).
18. K. Szot, W. Speier, S. Cramm, J. Herion, Ch. Freiburg, R. Waser, M. Pawelczyk, and W. Eberhardt, *J. Phys. Chem. Solids* **57,** 1765–1775 (1996).
19. O. Sørensen, Ed., "Nonstoichiometric Oxides." Academic Press, New York, 1981.
20. Ph. Ghosez, J.-P. Michenaud, and X. Gonze, *Phys. Rev. B* **58,** 6224–6240 (1998).
21. M. Neuman, G. Borstel, C. Scharfschwerdt, and M. Neuman, *Phys. Rev. B*, 10623 (1992).
22. J. F. Banfield and D. R. Veblen, *Am. Mineral.* **17,** 545 (1992).